# Hyperspectral mapping of lithium-bearing micas in Variscan Li bearing granite systems using Al-OH spectral shifts and multivariate analysis

L. Babedi[1]., R. Fitzpatrick[1]., R. Shail[1], J. Strongman[2], F. Wall[1]

[1] Critical Minerals Challenge Centre, Camborne School of Mines, University of Exeter, Penryn Campus, Penryn TR10 9FE, United Kingdom

[2] Petrolab Ltd, Redruth, United Kingdom

## Abstract

This study evaluates hyperspectral imaging integrated with multivariate statistical analysis for the discrimination of Li-bearing micas within ten Variscan Li bearing granite samples. Hyperspectral image cubes were processed using per-pixel Al-OH absorption feature extraction within the 2180-2240 nm electromagnetic radiation spectral region, enabling classification into Li-mica, muscovite-like mica, and Fe/Mg-rich mica populations based on diagnostic wavelength shifts. Mineralogical observations were supported using quantitative mineralogical datasets and spectral reference libraries. Principal Component Analysis (PCA), Hierarchical Cluster Analysis (HCA), and Partial Least Squares Discriminant Analysis with Variable Importance in Projection (PLS-DA-VIP) were used to evaluate spectral variability and identify dominant wavelengths controlling mica discrimination. The Al-OH region near 2190-2220 nm is the principal discriminator of mica chemistry, while secondary OH/$H_2O$ absorption regions also contribute significantly to classification performance. The workflow shows the potential of hyperspectral mineral mapping as a scalable approach for lithium exploration, geometallurgical domaining, and sustainable critical mineral resource evaluation.

# Introduction

The demand for battery materials such as lithium which has emerged as a cornerstone of modern energy storage technologies has seen an unprecedented increase in recent years as the global energy transitions towards low-carbon energy systems (Greim et al., 2020). Currently, the electric vehicle and energy storage sectors are predominantly producing batteries based on lithium-ion technologies due to higher energy density, long cycle life, and technological maturity, resulting in an increased global lithium demand (Greim et al., 2020; International Energy Agency (IEA), 2021). This has seen Europe and the United Kingdom having renewed interest in their lithium bearing granites and associated systems as a strategic component of future critical mineral supply chains (British Geological Survey (BGS), 2020; European Commission, 2023). Such moves highlight that exploration, resource evaluation, geometallurgical domaining and sustainable development of these emerging lithium resources require rapid, scalable, and cost-effective mineral characterization technologies.

For several decades, short-wave infrared (SWIR) reflectance spectroscopy has been considered a powerful and rapid tool in geoscience due to its ability to link changes in mineral chemistry to vibrational absorption features (Duke, 1994; Dalm et al., 2017). Hunt (1977) and Clark and Roush (1984) reported that SWIR region absorption signals enable the technique to effectively characterise hydroxyl-bearing minerals. Furthermore, Clark et al. (1990) stated that local bonding environments of structural hydroxyl groups in phyllosilicates strongly influences these absorption features. Tracing octahedral substitutions among mica minerals has been possible due to the sensitivity of the Al-OH feature (near 2200 nm) to site occupancy which influences the wavelength position of the absorption minimum (Duke, 1994, Dalm et al., 2017). The octahedral substitution of Li, Fe and Mg in micas has been associated with the observed shifts in the Al-OH feature towards either shorter or longer wavelengths (Laukamp et al., 2011; Cardoso-Fernandes et al., 2020). The increasing use of hyperspectral techniques in mining sectors is due to the capacity of spectral changes to serve as a diagnostic tool for differentiating mica populations at the pixel level (Laukamp et al., 2011; Cardoso-Fernandes et al., 2020; Meyer et al., 2022; Laukamp et al., 2021).

The use of hyperspectral technologies within lithium-bearing granite systems remains focused largely on exploration with limited applications on process mineralogical and geometallurgical interpretations of mica variability for systems like the Variscan Li bearing granites (Duke, 1994, Dalm et al., 2017, Cardoso-Fernandes et al., 2020; Meyer et al., 2022; Laukamp et al., 2021). This study uses Variscan granite samples to present a per-pixel hyperspectral workflow consisting of Al-OH adsorption extraction, spectral classification, multivariate statistical analysis, mineralogical validation and spatial mineral mapping. Collectively, these components of the workflow present a thorough evaluation of lithium-bearing mica variability and its geometallurgical implications. The integration of these approaches provides a statistically robust framework for linking spectral variability with mineralogical complexity, thereby supporting future geometallurgical characterization and beneficiation strategies for Variscan lithium-bearing granites.

# Materials and Methods

This study uses ten samples from Variscan lithium-bearing granites to capture the mineralogical variability associated with Li-bearing granite systems. The sample suite encompasses a range of lithological and mineralogical characteristics representative of different stages of granite evolution within the Variscan orogen, providing a suitable dataset for evaluating the hyperspectral response of white mica assemblages. Quantitative mineralogical analyses were conducted at Petrolab Ltd using a scanning electron microscopy (SEM) that uses the ZEISS Mineralogic Mining 1 automated mineral characterization system (Figure 1a-b). Hyperspectral images were collected at the University of Exeter's Camborne School of Mines (CSM) using a HySpex Baldur S-384N short-wave infrared (SWIR) hyperspectral imaging system with Prediktera Breeze software (version 2026.1.0). This system is integrated into the Comex LSX-400-MAX multi-sensor system, which also includes optical (RGB), Short-Wave Infrared (SWIR), X-Ray Fluorescence (XRF), and X-Ray Transmission (XRT) sensors for advanced mineral characterization and sorting applications. Hyperspectral image cubes were imported into Python and converted into three-dimensional data arrays consisting of spatial (x and y) and spectral dimensions. Prior to spectral analysis, each image

cube was visually inspected and cropped to remove conveyor belt edges and other non-sample regions. Cropping was performed using manually defined boundaries to ensure that only pixels representing the granite samples were retained for subsequent analysis. Reference spectra for muscovite, lepidolite and polylithionite were obtained from the United States Geological Survey (USGS) spectral library and compared across the full short-wave infrared region. The Al-OH absorption feature was extracted from the preprocessed hyperspectral data to characterize mica compositional variability. Only spectra exhibiting a diagnostic Al-OH absorption feature within the predefined wavelength interval were retained for subsequent analysis, thereby excluding non-mica pixels from wavelength classification. Multivariate statistical analyses (Principal Component Analysis (PCA) and Hierarchical Cluster Analysis (HCA)) and machine learning supervised models (Partial Least Squares Discriminant Analysis (PLS-DA)) were applied to investigate spectral variability within the hyperspectral dataset and to identify relationships between spectral responses and mica compositional differences.

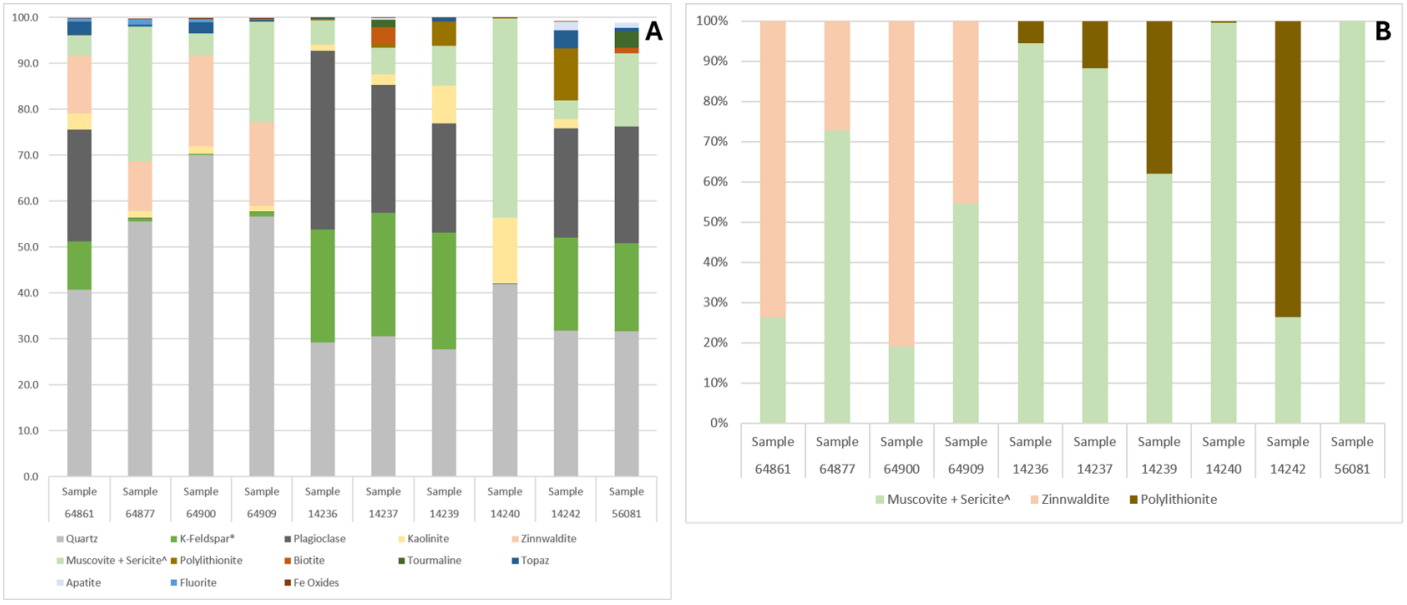


**Figure 1:** Quantitative modal mineralogy of the Variscan granite samples investigated.

# Results and discussion

## Al-OH absorption variability

The Al-OH adsorption feature was isolated from the Standard Normal Variate (SNV) -corrected spectra using the continuum removal method, allowing for mica compositional variation tracking of the Variscan granites. Duke (1994), Laukamp et al. (2011) and Meyer et al. (2022) recognized that the position of the Al-OH absorption feature (near 2200 nm) for dioctahedral white micas is directly controlled by octahedral cation substitutions and the local hydroxyl bonding environment. Most samples show dominant Al-OH absorption populations between approximately 2200 and 2220 nm, consistent with muscovite-rich white mica assemblages, whereas several samples contain shorter wavelength populations indicative of Li-bearing mica domains (Figure 2). In

contrast, absorption populations extending towards 2230 to 2240 nm are characteristic of Fe-rich lithium micas. These wavelength variations are controlled by differences in octahedral cation composition within the white mica group. Muscovite, with the ideal formula $KAl_2(AlSi_3O_{10})(OH)_2$, contains Al-dominated octahedral sites, whereas polylithionite, $KLi_2AlSi_4O_{10}(F,OH)_2$, and zinnwaldite, $KLiFe^{2+}Al(AlSi_3O_{10})(F,OH)_2$, contain increasing proportions of Li and Fe. The resulting changes in the local hydroxyl bonding environment shift the Al-OH absorption minimum, with Li-rich compositions occurring at shorter wavelengths and Fe-rich compositions at longer wavelengths (Duke, 1994; Laukamp et al., 2011; Meyer et al., 2022).

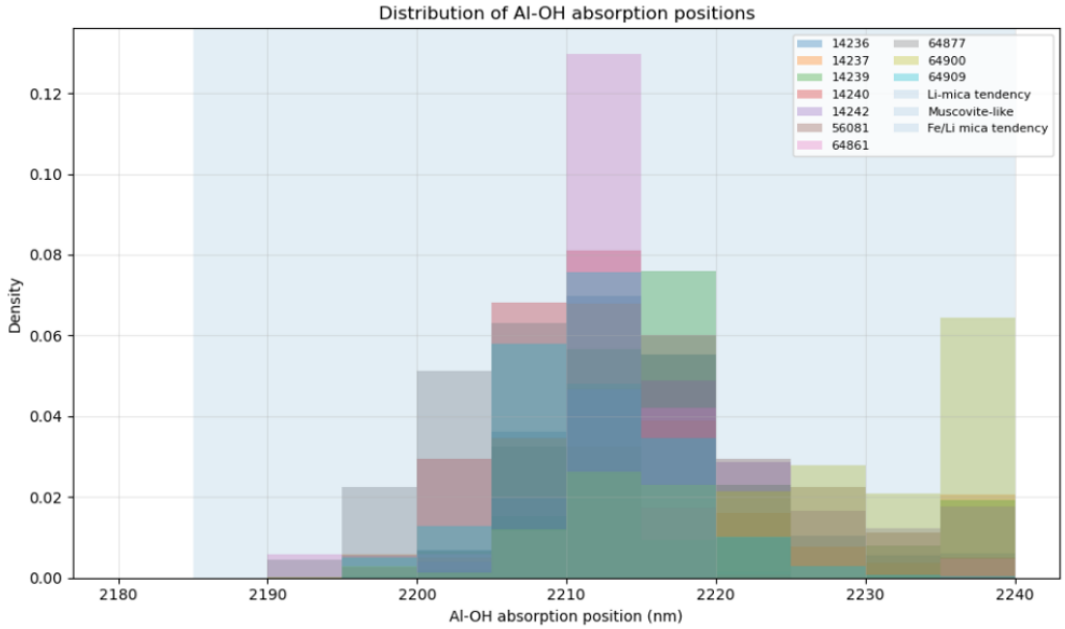


**Figure 2:** Distribution of Al-OH absorption positions derived from hyperspectral data. Distinct absorption populations indicate compositional variability among white micas, with shorter wavelengths corresponding to Li-rich micas and longer wavelengths reflecting muscovite-like and Fe/Mg-enriched mica compositions

## Relationship between hyperspectral absorption features and zinnwaldite abundance

The integration of hyperspectral and automated mineralogical datasets provides an opportunity to evaluate whether diagnostic spectral parameters respond systematically to variations in lithium-bearing mica abundance. Among the investigated Variscan granites, zinnwaldite-bearing samples exhibit a progressive increase in both the mean Al-OH and $H_2O$ absorption positions with increasing mineral abundance (Figure 3a-b). Figure 3 compares the mean Al-OH and $H_2O$ absorption positions with zinnwaldite abundance determined by automated mineralogy. Both spectral parameters show positive relationships with increasing zinnwaldite content. The mean Al-OH position increases from approximately 2208.5 nm in samples containing 10.9 wt.% zinnwaldite to 2225.9 nm in the sample containing 20 wt.% zinnwaldite (Figure 3a). A similar trend is observed for the $H_2O$ absorption position, which increases from 1928.2 to 1930.6 nm over the same range of zinnwaldite abundance (Figure 3b). The coefficients of determination ($R^2 = 0.62$ for Al-OH and $R^2 = 0.76$ for $H_2O$) indicate that both absorption features respond to changes in

zinnwaldite abundance, although the relationships are not statistically significant ($p > 0.05$). This is expected given that only four samples contain measurable zinnwaldite.

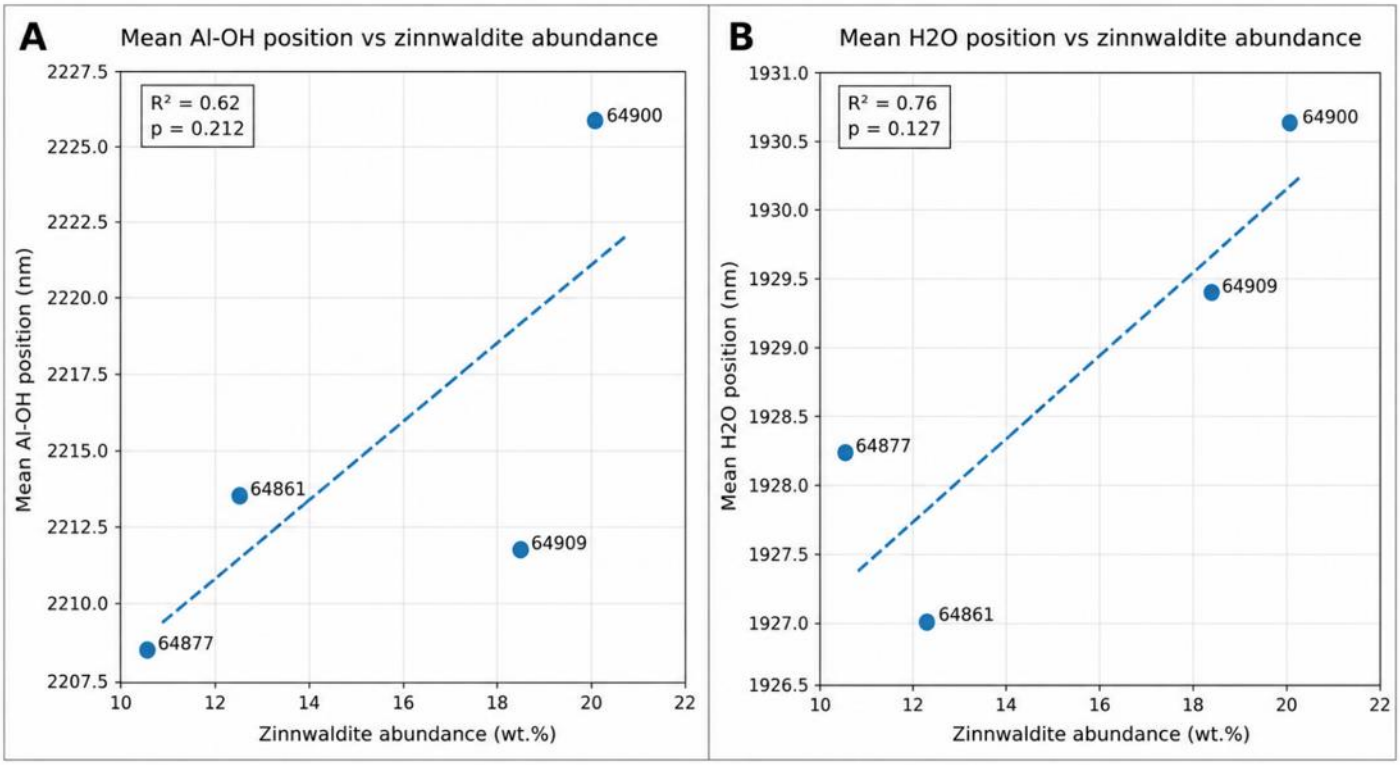


**Figure 3:** Relationship between hyperspectral absorption positions and zinnwaldite abundance determined by automated mineralogy. Mean Al-OH absorption position as a function of zinnwaldite abundance (A). Mean $H_2O$ absorption position as a function of zinnwaldite abundance (B). Dashed lines represent linear regression fits, with the corresponding coefficients of determination ($R^2$) and p-values shown on each plot.

The results observed here are consistent with these studies (Laukamp et al., 2011; Cardoso-Fernandes et al., 2021, Meyer et al., 2022), although the present work extends this relationship by comparing hyperspectral parameters directly with quantitative mineralogical measurements. The results indicate that increasing zinnwaldite abundance is accompanied by systematic changes in both hydroxyl- and water-related absorptions. However, the scatter between samples suggests that zinnwaldite abundance is not the only factor controlling the spectral response. Differences in crystal chemistry, mineral associations and the coexistence of muscovite-sericite and polylithionite are also likely to influence the position of these absorption features. Consequently, interpretation of Al-OH and $H_2O$ absorption positions should consider the complete white mica assemblage rather than individual lithium-bearing mica species. The agreement between the hyperspectral trends and the automated mineralogical data indicates that these spectral parameters provide useful proxies for compositional variation within the Variscan lithium-bearing mica assemblages.

## Multivariate analysis of spectral variability

Principal component analysis (PCA) evaluated the dominant sources of spectral variability within the hyperspectral dataset. The first two principal components explained 75.10% of the total variance, with PC1 and PC2 accounting for 62.39% and 12.71%, respectively (Figure 4). The majority of samples occupy distinct regions of the score plot, indicating that the spectral variability is systematic rather than randomly distributed. Samples 64900 and 64909 occur at negative PC1 values, whereas samples 14239 and 14242 are located towards the positive end of PC1. Samples 14236, 14237, 64861 and 56081 occupy intermediate positions, suggesting greater similarity in their spectral responses. Multivariate analyses of hyperspectral data have previously been useful to separate hydrothermal alteration and lithium-bearing pegmatites, where PCA resolved differences in white mica chemistry and mineral assemblages (Laukamp et al., 2021; Cardoso-Fernandes et al., 2021). Dalm et al. (2017) demonstrated that mineralogical variables derived from hyperspectral imagery, including white mica chemistry and crystallinity, provide an effective basis for multivariate classification of ore types.

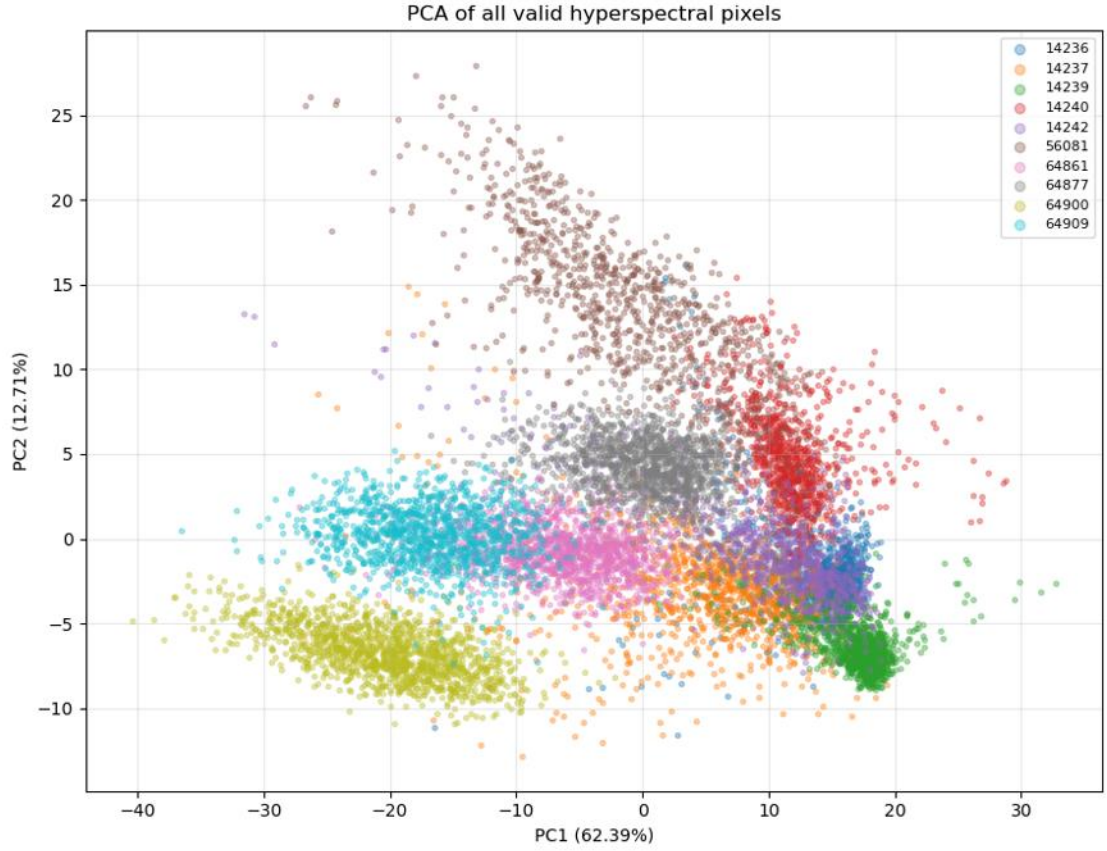


**Figure 4:** Principal component analysis (PCA) score plot of hyperspectral pixels from the investigated Variscan granite samples.

Figure 5 shows that the largest loading values occur near 1900 and 2200 nm. These wavelengths correspond to the $H_2O$ and Al-OH absorption features of white micas (Hunt, 1977; Clark et al., 1990). Loading values outside these regions vary only slightly. The separation of samples in Figure

8 is therefore associated mainly with changes in these two absorption features. Similar relationships between PCA loadings and white mica absorptions were reported by Laukamp et al. (2011).

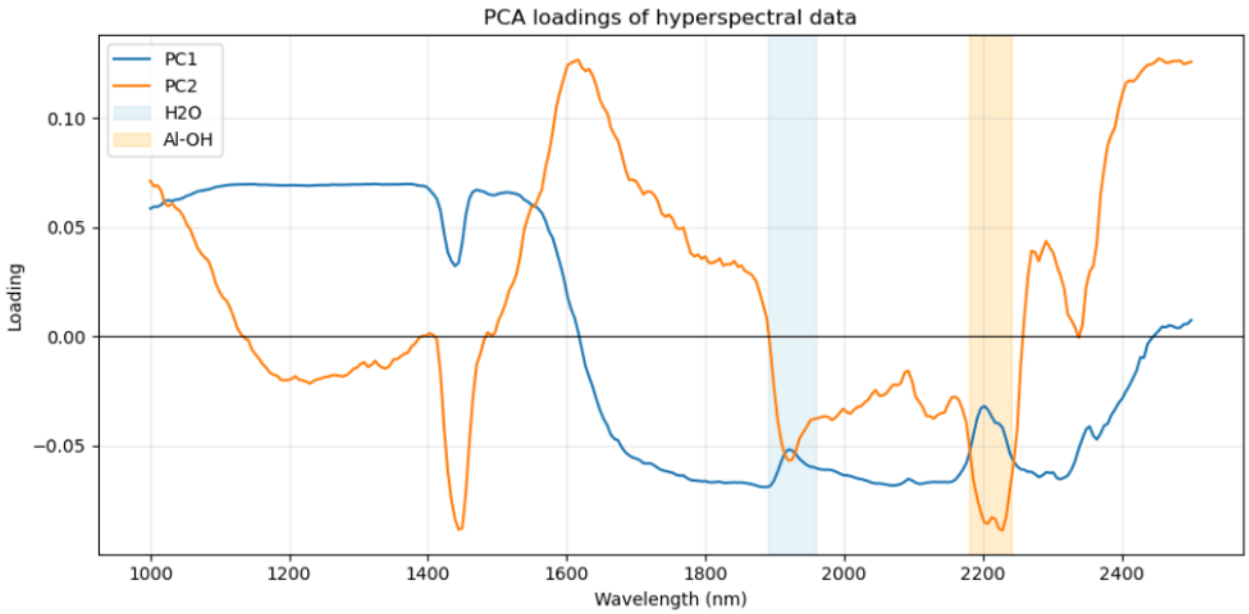


**Figure 5:** PCA loading spectra showing the contribution of individual wavelengths to PC1 and PC2. Shaded regions indicate the $H_2O$ and Al-OH absorption features.

Hierarchical cluster analysis (HCA) identified four major spectral clusters from the hyperspectral dataset (Figure 6). Comparison with the automated mineralogical data shows that each cluster is characterised by a distinct white mica assemblage (Figure 1). Cluster 1 contains the highest average polylithionite abundance together with moderate muscovite-sericite. Cluster 2 is characterised by the highest average zinnwaldite content. Cluster 3 contains mixed muscovite-sericite and zinnwaldite, whereas Cluster 4 is dominated by muscovite-sericite with negligible lithium-bearing mica. Although the clustering was performed exclusively on hyperspectral data, the resulting groups correspond closely with the mineralogical compositions determined independently by automated mineralogy. Similar relationships between hyperspectral clustering and mineralogical variability have been reported for drill core characterisation and process mineralogy applications, where multivariate analysis provides an effective means of identifying geometallurgical domains (Dalm et al., 2017). The agreement between PCA, HCA and automated mineralogy indicates that the hyperspectral dataset captures compositional variability within the white mica population rather than differences arising from random spectral noise. The first-order separation is controlled by diagnostic hydroxyl absorptions, while the subsequent clustering reflects differences in mica assemblages identified independently by SEM-based mineralogical analysis.

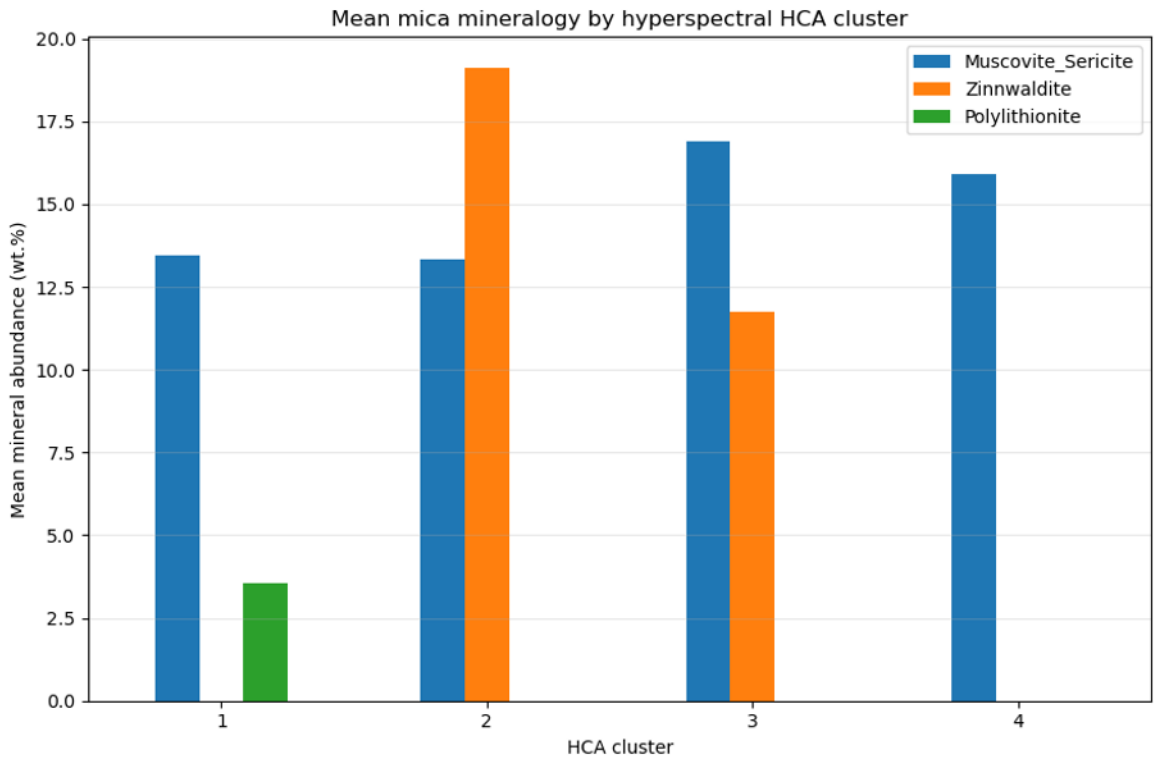


**Figure 6:** Mean abundances of muscovite-sericite, zinnwaldite and polylithionite within the hyperspectral HCA clusters determined from automated mineralogical analysis.

## PLS-DA classification and identification of diagnostic wavelengths

PLS-DA was used to evaluate the ability of the hyperspectral data to discriminate between the three white mica spectral populations defined from the Al-OH absorption positions. The confusion matrix (Figure 7a) shows that muscovite-like spectra were classified with the highest accuracy, with 1410 correctly classified observations. Misclassification within this class occurred predominantly towards the Fe/Li mica tendency class (163 observations), whereas no muscovite-like spectra were assigned to the Li-mica tendency class. In contrast, the Li-mica tendency class showed the lowest classification accuracy, with only 31 correctly classified observations and a substantial proportion assigned to the muscovite-like class. The Fe/Li mica tendency class showed intermediate performance, with 1017 correctly classified observations and relatively limited confusion with the Li-mica tendency class. The classification pattern indicates that the principal source of uncertainty occurs between neighbouring spectral populations rather than between compositionally distinct end members. Similar behaviour has been reported for hyperspectral classification of alteration minerals, where overlapping spectral characteristics produce gradual transitions between mineral classes instead of discrete boundaries (Barker and Rayens, 2003; Cardoso-Fernandes et al., 2021).

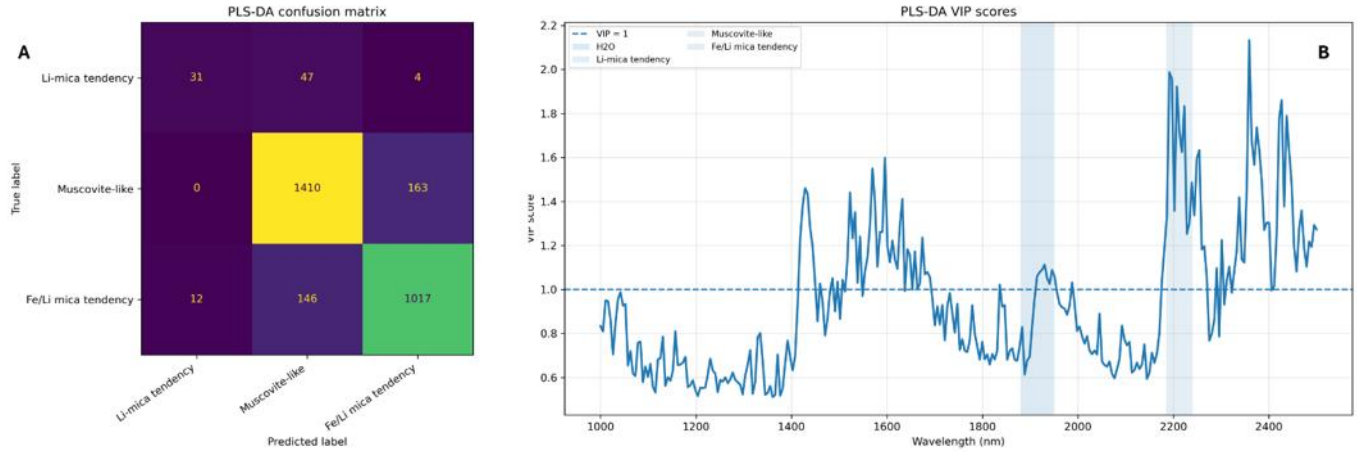


**Figure 7:** PLS-DA confusion matrix showing the classification performance of Li-mica, muscovite-like, and Fe/Li mica populations (A). Variable importance in projection (VIP) scores highlighting the spectral regions controlling white mica discrimination, with the Al-OH absorption region near 2200 nm identified as the most diagnostic spectral feature (B).

The corresponding VIP scores identify the spectral regions contributing most to class discrimination (Figure7b). Wavelengths exceeding the commonly adopted threshold of VIP > 1 occur predominantly within the 1400–1650 nm, 1900–1950 nm and 2200–2250 nm regions, with additional contributions observed beyond 2350 nm. These intervals coincide with hydroxyl- and molecular water-related absorptions that dominate the SWIR response of white micas (Clark et al., 1990; Hunt, 1977). The highest VIP values are associated with the Al-OH absorption region centred near 2200 nm and the longer wavelength absorption features above 2350 nm, indicating that these regions contain the greatest discriminatory information for separating the spectral populations investigated. In comparison, spectral regions with VIP values below unity contributed little to the classification model and therefore contain limited information for distinguishing between the three white mica groups. The agreement between the VIP profile and the principal absorption features identified in Sections 3.1 and 3.2 indicates that the classification model is driven by mineralogically meaningful spectral variation rather than statistical artefacts.

# Geometallurgical implications for Variscan lithium granites

The combination of hyperspectral imaging, multivariate statistics and supervised machine learning provides a rapid and non-destructive framework for delineating mineralogical variability within Variscan lithium granites. This becomes important for developing geometallurgical workflows that seek to improve lithium extraction from the mica rich Variscan granites. Lithium bearing granites are characterized by variability in the distribution, abundance and chemistry of micas, thus controlling the deportment and processing performance. Establishing a quantitative relationship between these geological differences and metallurgical performance remains the cornerstone of predictive geometallurgy (Lotter et al., 2018). The current illustration of discriminating Li-rich micas from muscovite and Fe-rich mica populations represents a valuable step towards the definition of geometallurgical domains. Overall, this study demonstrates that hyperspectral imaging integrated with machine learning represents a powerful geometallurgical tool for Variscan lithium granites. The workflow links hyperspectral measurements with mineralogical composition

and lithium deportment. Integration with automated mineralogy, quantitative mineral chemistry and flotation response will enable direct comparison between spectral variability and metallurgical behaviour. Application of the workflow to larger datasets will allow its suitability for geometallurgical characterisation of lithium-bearing granite deposits to be assessed.

# Conclusions

The hyperspectral analyses presented in this study resolved compositional variability within lithium-bearing mica assemblages from ten Variscan granites. The Al-OH absorption feature separated muscovite-like, Li-rich and Fe/Li-rich white mica populations, while PCA and HCA identified distinct spectral groups that were consistent with automated mineralogical data. PLS-DA showed that the principal discriminatory wavelengths were concentrated within the diagnostic $H_2O$ and Al-OH absorption regions. Comparison with automated mineralogy showed that variations in spectral responses reflected changes in white mica composition rather than mineral abundance alone. The workflow combines per-pixel hyperspectral analysis with multivariate statistics and mineralogical validation, providing a rapid approach for characterising lithium-bearing granites. The methodology is applicable to drill core characterisation and geometallurgical domaining where rapid assessment of white mica variability is required.

# Acknowledgements

The authors acknowledge the UK Research and Innovation (UKRI) for financial support through the Critical Minerals and Circular Economy Centre (CMCC). The authors thank James Strongman and Petrolab Ltd. for providing the Variscan granite samples and undertaking the automated mineralogical analyses. The authors also acknowledge the Camborne School of Mines, University of Exeter, for access to hyperspectral imaging facilities and analytical infrastructure used in this study. The constructive discussions and technical support provided by colleagues within the CMCC project are gratefully acknowledged.

# References

Barker, M. and Rayens, W., 2003. Partial least squares for discrimination. Journal of Chemometrics, 17(3), pp.166 to 173.

British Geological Survey (BGS), 2020. The Potential for Lithium in the UK. Raw Materials for Decarbonisation. Nottingham: British Geological Survey.

Cardoso-Fernandes, J., Teodoro, A.C., Lima, A. and Roda-Robles, E., 2020. Semi-automatization of support vector machines to map lithium (Li) bearing pegmatites. Remote Sensing, 12(14), 2319.

Cardoso-Fernandes, J., Silva, J., Perrotta, M.M., Lima, A., Teodoro, A.C., Ribeiro, M.A., Dias, F., Barrès, O., Cauzid, J. and Roda-Robles, E., 2021. Interpretation of the reflectance spectra of lithium (Li) minerals and pegmatites: A case study for mineralogical and lithological identification in the Fregeneda-Almendra area. Remote Sensing, 13(18), 3688.

Clark, R.N. and Roush, T.L., 1984. Reflectance spectroscopy: Quantitative analysis techniques for remote sensing applications. Journal of Geophysical Research, 89(B7), pp.6329 to 6340.

Clark, R.N., King, T.V.V., Klejwa, M., Swayze, G.A. and Vergo, N., 1990. High spectral resolution reflectance spectroscopy of minerals. Journal of Geophysical Research, 95(B8), pp.12653 to 12680.

Dalm, M., Buxton, M.W.N. and van Ruitenbeek, F.J.A., 2017. Discriminating ore and waste in a porphyry copper deposit using short-wavelength infrared (SWIR) hyperspectral imagery. Minerals Engineering, 105, pp.10-18.

Duke, E.F., 1994. Near infrared spectra of muscovite, Tschermak substitution, and metamorphic reaction progress: Implications for remote sensing. Geology, 22(7), pp.621-624

European Commission, 2023. Study on the Critical Raw Materials for the EU 2023: Final Report. Luxembourg: Publications Office of the European Union.

Greim, P., Solomon, A.A. and Breyer, C., 2020. Assessment of lithium criticality in the global energy transition and addressing policy gaps in transportation. Nature Communications, 11, 4570.

Hunt, G.R., 1977. Spectral signatures of particulate minerals in the visible and near infrared. Geophysics, 42(3), pp.501 to 513.

International Energy Agency (IEA), 2021. World Energy Outlook 2021. Paris: International Energy Agency.

Laukamp, C., Cudahy, T., Thomas, M., Jones, M., Cleverley, J.S. and Oliver, N.H.S., 2011. Hydrothermal mineral alteration patterns in the Mount Isa Inlier revealed by airborne hyperspectral data. Australian Journal of Earth Sciences, 58(8), pp.917-936

Laukamp, C., LeGras, M. and Lau, I.C., 2021. Hyperspectral Proximal Sensing Instruments and Their Applications for Exploration Through Cover. In: R. Crocombe, P. Leary and B. Kammrath, eds. Portable Spectroscopy and Spectrometry. Wiley.

Lotter, N.O., Baum, W., Reeves, S., Arrué, C. and Bradshaw, D.J., 2018.The business value of best practice process mineralogy. Minerals Engineering, 116, pp.226-238.

Meyer, J.M., Holley, E.A. and Kokaly, R.F., 2022. Hyperspectral remote sensing of white mica: A review of imaging and point-based spectrometer studies for mineral resources, with spectrometer design considerations. Remote Sensing of Environment, 275, 113000.